J Comput Electron (2012) 11:8–13
DOI 10.1007/s10825-012-0390-2

Mesoscale modeling of phononic thermal conductivity of porous Si: interplay between porosity, morphology and surface roughness

Giuseppe Romano · Aldo Di Carlo · Jeffrey C. Grossman

Published online: 29 February 2012

Abstract In this work we compute the effective thermal conductivity of porous Si by means of the phonon Boltzmann transport equation. Simulations of heat transport across aligned square pores reveal that the thermal conductivity can be decreased either by increasing the pore size or decreasing the pore spacing. Furthermore, by including the surface specularity parameter we show that the roughness of the pore walls plays an important role when the pore size is comparable with the phonon mean free path, because to the increase in the surface-to-volume ratio. Thanks to these results, in qualitatively agreement with those obtained with Molecular Dynamics simulations, we gained insights into the scaling of thermal properties of porous materials and interplay between disorder at different length scales. The model, being based on a flexible multiscale finite element context, can be easily integrated with electrical transport models, in order to optimize the figure of merit ZT of thermoelectric devices.

Keywords Thermoelectrics · Boltzmann · Thermal conductivity

G. Romano · J.C. Grossman (✉)
Department of Materials Science and Engineering, Massachusetts Institute of Technology, 77 Massachusetts Avenue, Cambridge, MA 02139, USA
e-mail: jcg@mit.edu

G. Romano
e-mail: romanog@mit.edu

A. Di Carlo
Department of Electronics Engineering, University of Rome "Tor Vergata", Via del Politecnico 1, 00133, Rome, Italy
e-mail: aldo.dicarlo@uniroma.2it

1 Introduction

Thermoelectric materials have gained much attention recently due to their ability to convert directly heat into electricity and provide efficient solid-state cooling [1, 2]. The efficiency of such materials can be described in terms of the dimensionless figure-of-merit $ZT = \sigma S^2 T/\kappa$, where σ is the electrical conductivity, S the Seebeck coefficient, T the temperature and κ the total thermal conductivity. Ideally, a thermoelectric material should be a "phonon glass—electron crystal" [3, 4], namely it should have low thermal conductivity and high electrical conductivity. Optimizing the performance of real thermoelectric materials (maximizing S and the ratio σ/κ) is particularly challenging in bulk materials because all three quantities are interrelated. In a large majority of materials and systems, an increase in σ is accompanied by a decrease in S, and σ is proportional to the electronic contribution to κ from the Widemann-Franz law. There are, however, many possibilities that exploit special features of unusual energy band characteristics and/or quantum effects from reduced dimensionality [5] (such as the tuning of electronic bandgaps and density of states, or the confinement of phonons) to improve performance in thermoelectric materials. The electronic structure may be controlled through materials choice [6] tailored superlattices [7], and nanostructuring [5] in order to independently tune S, σ and κ. As an example of this latter category, micro and nano-porous materials have gained recent and growing attention for applications in thermoelectrics, owing to their ability to decouple to some extent the electrical and thermal transport [8–12]. Indeed, by carefully choosing the porosity and surface-to-volume ratio, it has been both theoretically predicted [10] and experimentally demonstrated [8, 9] that nanoporous thin films can block heat remarkably well, with relatively little degradation in the electrical conductivity. Molecular Dynamics (MD) simulations show that pores

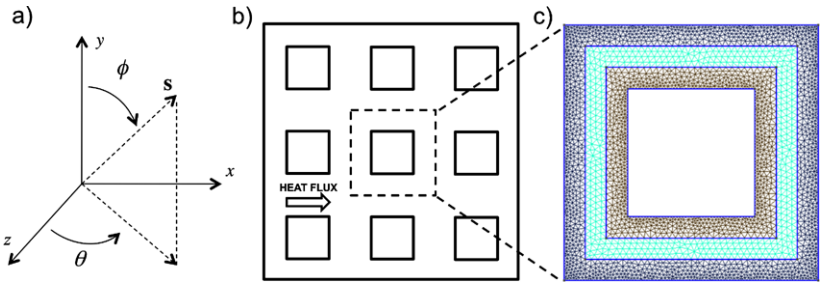

Fig. 1 (**a**) The vector **s** in spherical coordinates. (**b**) Schematic of the periodic nanoporous material. Heat travels along the x-direction in our simulations. (**c**) The unit cell used in the simulation. The most inner and outer regions have a finer mesh, in order to improve the accuracy on the flux conservation

as small as several nanometers in diameter are able to lower the phononic thermal conductivity (PTC) up to two orders of magnitude [11]. Recently, it has been shown that the surface roughness and the thickness of the film can significantly enhance the phonon scattering, leading to a further reduction in the PTC [12]. However, while molecular dynamics provides important information about phonon dynamics at the nanoscale, they become computational intractable when dealing with heat transport across mesoscale materials and devices.

In this work we have computed the effective thermal conductivity of porous Si across multiple length scales by means of the steady-state Phonon Boltzmann Transport Equation (PBTE), under the gray medium approximation [15]. According to the experimental results [8], we found that classical size effect still plays an important role when the periodicity is larger than the phonon mean free path (*mfp*). In investigating the interplay between the porosity and surface roughness, we found that the surface roughness becomes important for high porosities and low pore sizes in terms of phonon *mfp*, namely for high surface-to-volume ratio. Furthermore, assuming completely diffuse pore walls, pore size and spacing have been varied in order to understand their effect on the PTC. We found that the PTC can be lowered by either decreasing the pore spacing or increasing the pore size, according to MDs results [11]. The model has been discretized by means of the Discontinuous Galerkin method and integrated in the platform tool for multiscale modeling TiberCAD [13, 14]. This will foster the combined modeling of heat and electrical transport, in order to provide an effective optimization of the figure of merit ZT.

2 Model

As shown in Fig. 1, the simulation domain consists of a pore embedded in a Si plane with length L. The heat flux is enforced to flow along the x-direction due to an applied temperature difference ΔT. Boundary conditions will be discussed later in the text. Heat transport is modeled by means of the PBTE under the relaxation time and gray medium approximation [15]. A rigorous treatment should include the full phonon dispersion in the calculation [16]. However, previous studies has successfully employed the gray model for heat transport in microstructures, showing that it is still a good a approximation [17–22]. The PBTE to be solved is

$$v_g \mathbf{s} \cdot \nabla I = \frac{I - I_0}{\tau} \tag{1}$$

where I is the energy density of phonons per solid angle, I_0 is the equilibrium energy density, $v_g = 8.433 \cdot 10^3$ m/s is the average group velocity and $\mathbf{s}$ is the direction in which phonons propagate, which is given by

$$\mathbf{s} = \begin{pmatrix} \sin(\theta)\sin(\phi) \\ \sin(\theta)\cos(\phi) \\ \cos(\theta) \end{pmatrix}$$

In (1) τ is the scattering time, which is computed by $\tau = (3\kappa_{bulk})/(v_g^2 C)$, where $\kappa_{bulk} = 150$ W/(mK) is the Si bulk thermal conductivity and $C = 1.66 \cdot 10^6$ J/(m^{3}K) is the Si volumetric heat capacity. Energy conservation is ensured by the following average on the solid angle

$$I_0 = \frac{1}{4\pi} \int_{4\pi} I \, d\Omega \tag{2}$$

If we assume that the temperature gradient across the unit cell is small, the heat capacity can be approximated as temperature independent. The temperature map is then computed by

$$4\pi I_0 = C(T - T_0) \tag{3}$$

where $T_0 = 300$ K is the reference temperature, whereas the expression for the thermal flux reads as

$$\mathbf{J} = \int_{4\pi} I \mathbf{s} d\Omega \tag{4}$$

The PTC is then calculated by Fourier's law, i.e.

$$\kappa_{eff} = \frac{L}{\int_0^L [T(0, y) - T(L, y)] dy} \int_0^L J_x(0, y) dy \tag{5}$$

where J_x is the thermal flux along the direction where the temperature is applied. Equation (5) includes an average of

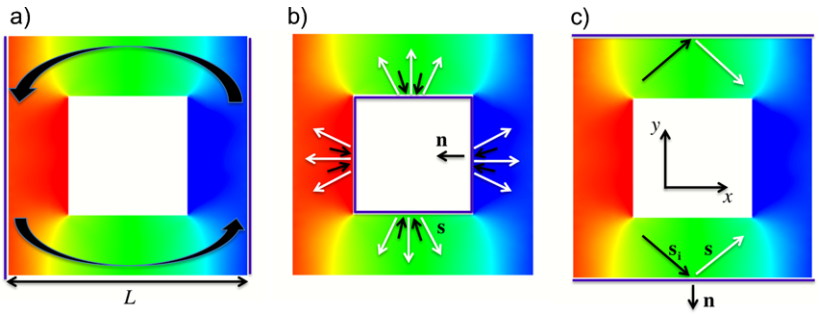

Fig. 2 Schematic view for (**a**) periodic, (**b**) specular and (**c**) diffuse boundary conditions

the thermal flux and temperature along the direction perpendicular to the heat flux. The first guess for I_0 is given by a Fourier simulation,

$$\mathbf{J} = -\kappa_{bulk} \nabla T \tag{6}$$

which takes into account the applied temperature [23, 24]. Once the temperature map has been computed by (6), the initial value for the equilibrium energy density is given using (3).

The solid angle has been discretized in 32 polar angles and 8 azimuthal angles. The domain for θ is restricted to $(0, \pi/2)$ due to the symmetry of the system under consideration. The spatial discretization is based on a 2D unstructured Delaney mesh [25], which is refined around the pore and close to the external boundary, in order to enhance the accuracy on flux conservation. Equation (1) is discretized by means of the zeroth-order discontinuous Galerkin method, which is formally equivalent to the finite volume method, usually employed for discretization of the PBTE [26, 27]. Calculations are based on a module developed within the TiberCAD platform [13, 14]. For details related to the numerical implementation of (1), refer to [23].

3 Boundary conditions

In principle, to include the effect of the pore spacing, multiple pores should be included in the simulation domain. However, as our work focuses on the case of periodically aligned pores we may apply periodic boundary conditions leading to a remarkable reduction in the computational time. As depicted in Fig. 2, heat flux is enforced to flow along the x-direction and the thermal conductivity is computed for a unit cell composed by one pore. It can be proven that cell-cell interactions are taken into account if the following constraints are applied at the left and right sides [20, 28]

$$I(0, y, \mathbf{s}) - I_0(0, y, \mathbf{s}) = I(L, y, \mathbf{s}) - I_0(L, y, \mathbf{s}) \tag{7}$$

Equation (7) implies that the departure of the energy density from the equilibrium value is equal across the left and right side at each point along the y-direction. By integrating both sides of (7) and remembering that I_0 is isotropic, i.e. $\int_{4\pi} I_0 \mathbf{s} d\Omega = 0$, it is straightforward to show that the flux is conserved.

On the upper and lower side, we apply specular boundary conditions because of the symmetry (see Fig. 2b)

$$I_R(\mathbf{r}, \mathbf{s}) = I(\mathbf{r}, \mathbf{s_i}) \tag{8}$$

where $I_R(\mathbf{r}, \mathbf{s})$ is the energy density of phonons reflected at the surface and $\mathbf{s_i}$ is the phonon energy density propagating toward the boundary domain. The directions $\mathbf{s}$ and $\mathbf{s_i}$ are related to the following relationship

$$\mathbf{s_i} = \mathbf{s} - 2|\mathbf{s} \cdot \mathbf{n}|\mathbf{n} \tag{9}$$

where $\mathbf{n}$ is the normal to the surface where phonons are reflected. Pore walls are treated as being partially diffuse. When a surface is diffuse, e.g. because the roughness length is comparable with the phonons wavelength, phonons out coming from a boundary scattering do not bear information about their direction before the scattering event. The phonon density incoming into the domain along a given surface can be computed by an average of all phonons going toward that surface (see Fig. 2c), i.e.

$$I_D(\mathbf{r}, \mathbf{s}) = \frac{1}{\pi} \int_{\mathbf{s}\cdot\mathbf{n}>0} I(\mathbf{r}, \mathbf{s}) \mathbf{s} \cdot \mathbf{n} d\Omega \tag{10}$$

where I_D means the energy density of phonons being diffusively scattered and $\mathbf{s} \cdot \mathbf{n} > 0$ include all the direction pointing outside the domain. However, a real surface may be described by the surface specularity parameter p, which allows to span from the specular to the diffuse surface

$$I(\mathbf{r}, \mathbf{s}) = p I_R(\mathbf{r}, \mathbf{s}) + (1 - p) I_D(\mathbf{r}, \mathbf{s}) \tag{11}$$

The specularity parameter can be computed by the expression $p = \exp(16\pi^2\delta^2/\lambda^2)$ where δ is the roughness length and λ is the phonon wavelength [29–31].

4 Results

In absence of phonon classical size effects, the PTC can be computed by means of Fourier's law, which takes into

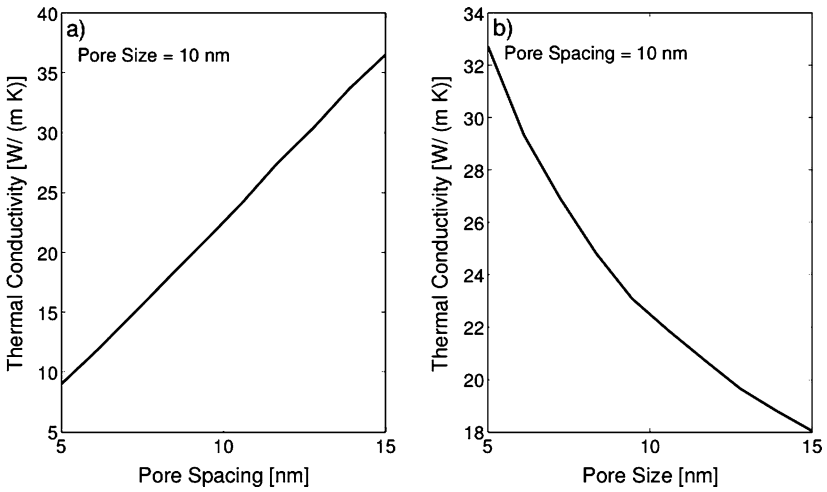

Fig. 3 (**a**) PTC vs pore spacing for a pore size of 10 nm, (**b**) PTC vs pore size for a pore spacing of 10 nm

account geometrical effect. For porosity $\phi < 0.4$ and for aligned cylindrical pores, PTC can be approximated by [32]

$$\kappa_{eff} = \kappa_{bulk} f(\phi) = \kappa_{bulk} \frac{1-\phi}{1+\phi} \tag{12}$$

Equation (12) can be used, as a good approximation, for square pores, as well [32]. Let us now include the phonon-pore scattering in the calculation by solving (1)–(2). As in previous work on nanoporous silicon [11], here the pore size and pore spacing have been varied in order to understand their effect on the PTC. The surface of the wall is assumed completely diffuse ($p = 0$). We first fix the pore size to $d_p = 10$ nm and allow the pore spacing to vary between $d_p = 5$ to $d_p = 15$ nm. As can be seen in Fig. 3a and as expected, the thermal conductivity decreases when the pore spacing decreases. This effect can be understood by noting that for low pore spacing the porosity, which is given by $\phi = (d_p^2)/(d_p^2 + d_s^2)$, increases leading to a reduction of the volume through which heat can travel. In Fig. 3b, results for fixed pore spacings are shown. In this case, the thermal conductivity decreases as the pore size increases. Indeed, for high pore size the surface-to-volume ratio, which is given by $\rho = (4d_p)/((d_p + d_s)^2)$, increases and, as a consequence, the phonon-pore scattering increases. The values shown in Fig. 3 are roughly one order of magnitude lower than the bulk value.

Next, we extend the range of variability of the unit cells, to multiple length scales and vary the specularity of the pores surface, mimicking changes in the surface roughness. The porosity varies from $\phi = 0.05$ to $\phi = 0.3$. The pore size spans from $d_p = 5$ nm to $d_p = 500$ nm, namely to almost ten times the phonon *mfp*. The surface specularity parameter associated with the pore walls goes from $p = 0$ to $p = 1$. We now consider the case where the porosity is fixed to $\phi = 0.3$ and compute the PTC for different pore size and p. Results are shown in Fig. 4. For pores larger than the phonon *mfp*,

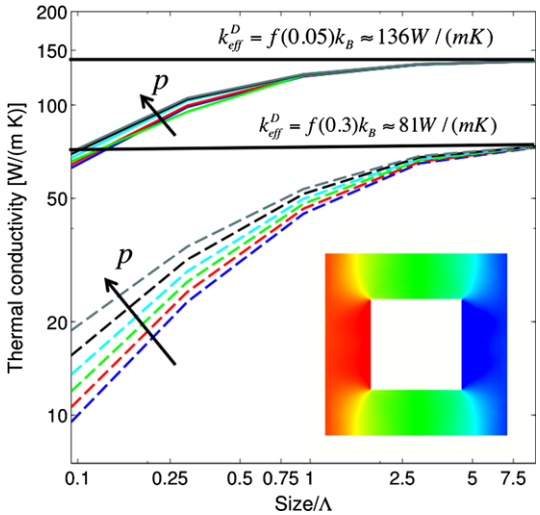

Fig. 4 PTC vs pore size, for different surface specularity parameter and porosity. In the inset the simulation domain is provided

the PTC converges to the value predicted by (12), recovering, therefore, the diffuse limit. However, for pore size larger than the phonon *mfp*, classical size effect are important, according to experimental data [8]. When the pore size becomes much smaller than the phonon *mfp*, heat transport becomes purely ballistic and the *view factor* becomes predominant [33]. In Fig. 5 thermal flux lines are shown for pore size (a) $d_p = 500$ nm (b) $d_p = 125$ nm and (c) $d_p = 30$ nm. For the latter case, phonons travel mostly through direct paths and materials acts as an array of nanowire rather than a porous material.

Let us now focus on the effect of the surface specularity parameter. When the pore size approaches the phonon *mfp*, the phonon-pore scattering "turns on" and the effect of the specularity becomes important, revealing therefore the importance of the effect of surface roughness for nanome-

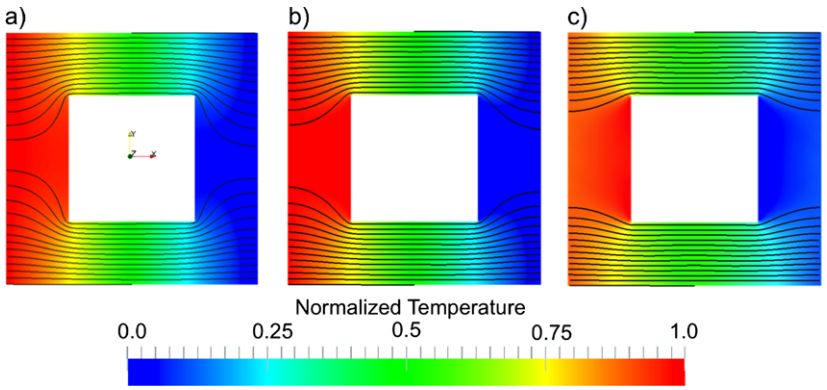

Fig. 5 Temperature map and thermal flux lines for porosity $\phi = 0.3$, $p = 0$ and for pore size (**a**) $d_p = 500$ nm, (**b**) $d_p = 125$ nm and (**c**) $d_p = 30$ nm. When the pore size approaches the phonon *mfp* phonon travel mostly through the direct path

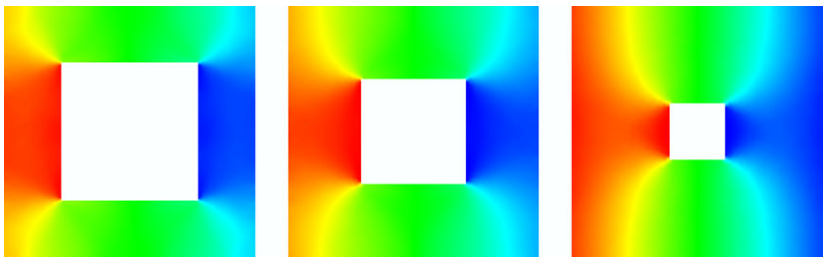

Fig. 6 Temperature map for $d_p = 16$ nm, $p = 0$ and porosity (**a**) $\phi = 0.05$, (**b**) $\phi = 0.175$ and (**c**) $\phi = 0.3$ (not in scale)

ter scale pores, in agreement with previous MD simulations [12]. This effect is due to the increase of the surface-to-volume ratio $\rho = \frac{4\phi}{d_p}$ which correlates with the phonon-pore scattering. The lowest value in the PTC is reached for a purely diffuse surface ($p = 0$) because the loss of information at the boundary introduces an additional disorder to the phonon trajectory. When the porosity becomes as small as 0.05, the surface-to-volume ratio decreases (as depicted in Fig. 6) and, as a consequence, the effect of the surface roughness becomes less important.

5 Conclusion

In this work we have used a Discontinuous Galerkin Method to solve the PBTE within the gray medium approximation for a porous material in order to compute heat transport across aligned pores. Studying the interplay between porosity and disorder across multiple length scales we found that surface roughness plays an important role when the pore size is comparable with the phonon *mfp*. Furthermore, by varying the pore spacing and size we have found the correlation between the PTC, the porosity and surface-to-volume ratio. The obtained trends are in agreement with MDs results. Both the ballistic and Fourier limit have been discussed. The presented approach, being based on a flexible finite element context, will easily allow to explore new areas of thermoelectricity optimization, such as different pore shapes, arrangement, 3D structure and will also permit the integration of carrier transport model (i.e. Drift-diffusion).

References

1. Majumdar, A.: Enhanced: thermoelectricity in semiconductor nanostructures. Science **303**, 777 (2004)
2. Zebarjadi, M., Esfarjani, K., Dresselhaus, M.S., Ren, Z.F., Chen, G.: Perspectives on thermoelectrics: from fundamentals to device applications. Energy Environ. Sci. **5**, 5147 (2011)
3. Snyder, G.: Complex thermoelectric materials. Nat. Mater. **7**, 105 (2008)
4. Minnich, A.J., Dresselhaus, M.S., Ren, Z.F., Chen, G.: Bulk nanostructured thermoelectric materials: current research and future prospects. Energy Environ. Sci. **2**, 466–479 (2009)
5. Hicks, L.D., Harman, T.C., Dresselhaus, M.S.: Use of quantum-well superlattices to obtain a high figure of merit from nonconventional thermoelectric materials. Appl. Phys. Lett. **3230** (1993)
6. Mahan, G.D., Sofo, J.O.: The best thermoelectric. Proc. Natl. Acad. Sci. **93**, 7436 (1996)
7. Humphrey, T.E., Linke, H.: Reversible thermoelectric nanomaterials. Phys. Rev. Lett. **94**, 096601 (2005)
8. Song, D., Chen, G.: Thermal conductivity of periodic microporous silicon films. Appl. Phys. Lett. **84**(5), 687 (2004)
9. Yu, J.-K., Mitrovic, S., Tham, D., Varghese, J., Heath, J.R.: Reduction of thermal conductivity in phononic nanomesh structures. Nat. Nanotechnol. **5**, 718 (2010)
10. Lee, J.-H., Galli, G.A., Grossman, J.C.: Nanoporous Si as an efficient thermoelectric material. Nano Lett. **8**, 3750 (2008)
11. Lee, J., Grossman, J., Reed, J.: Lattice thermal conductivity of nanoporous Si: Molecular dynamics study. Appl. Phys. Lett. **91**, 223110 (2007)
12. He, Y., Donadio, D., Lee, J.-H., Grossman, J.C., Galli, G.: Thermal transport in nanoporous silicon: interplay between disorder at mesoscopic and atomic scales. ACS Nano **5**, 1839 (2011)
13. Auf der Maur, M., Penazzi, G., Romano, G., Sacconi, F., Pecchia, A., Di Carlo, A.: The multiscale paradigm in electronic device simulation. IEEE Trans. Electron Devices **58**, 1425 (2011)
14. www.tibercad.org
15. Sparrow, E.M., Cess, R.D.: Radiation Heat Transfer. CRC Press, Boca Raton (1978)

16. Hao, Q., Chen, G., Jeng, M.-S.: Frequency-dependent Monte Carlo simulations of phonon transport in two-dimensional porous silicon with aligned pores. J. Appl. Phys. **106**, 114321 (2009)
17. Majumdar, A.: Microscale heat conduction in dielectric thin films. Trans. ASME, J. Heat Transf. **115**, 7 (1993)
18. Joshi, A.A., Majumdar, A.: Transient ballistic and diffusive phonon heat transport in thin films. J. Appl. Phys. **74**, 31 (1993)
19. Chen, G.: Nanoscale Energy Transport and Conversion: A Parallel Treatment of Elections, Molecules, Phonons, and Photons. Oxford Univ. Press, London (2005)
20. Yang, R.G., Chen, G.: Thermal conductivity modeling of periodic two-dimensional nanocomposites. Phys. Rev. B **69**, 195 (2004)
21. Liu, L.-C., Huang, M.-J.: Thermal conductivity modeling of micro- and nanoporous silicon. Int. J. Therm. Sci. **49**(9), 1547 (2010)
22. Chung, J.D., Kaviany, M.: Effects of phonon pore scattering and pore randomness on effective conductivity of porous silicon. Int. J. Heat Mass Transf. **43**, 521 (2000)
23. Romano, G., Di Carlo, A.: Multiscale electro-thermal modeling of nanostructured devices. IEEE Trans. Nanotechnol. **10**, 1285 (2011)
24. Romano, G., Auf der Maur, M., Pecchia, A., Di Carlo, A.: Handshaking multiscale thermal model of nanostructured devices. In: Proceedings of the 14TH International Workshop on Computational Electronics, p. 68 (2010)
25. Thompson, J.F., Soni, B.K., Weatherill, N.P.: Handbook of Grid Generation. CRC Press, Boca Raton (1999)
26. Murthy, J.Y., Mathur, S.R.: Computation of sub-micron thermal transport using an unstructured finite volume method. J. Heat Transf. **124**, 1176 (2002)
27. Murthy, J.Y., Mathur, S.R.: An improved computational procedure for sub-micron heat conduction. J. Heat Transf. **125**, 904 (2003)
28. Chen, G.: Thermal conductivity and ballistic-phonon transport in the cross-plane direction of superlattices. Phys. Rev. B **57**, 14958 (1998)
29. Ziman, J.M.: Electrons and Phonons. Oxford University Press, London (1985)
30. Soffer, S.B.: Statistical model for the size effect in electrical conduction. J. Appl. Phys. **38**, 1710 (1967)
31. Aksamija, Z., Knezevic, I.: Anisotropy and boundary scattering in the lattice thermal conductivity of silicon nanomembranes. Phys. Rev. B **82**(4), 045319 (2010)
32. Nan, C.-W., Birringer, R., Clarke, D.R., Gleiter, H.: Effective thermal conductivity of particulate composites with interfacial thermal resistance. J. Appl. Phys. **81**, 6692 (1997)
33. Prasher, R.: Transverse thermal conductivity of porous materials made from aligned nano and microcylindrical pores. J. Appl. Phys. **100**, 064302 (2006)